

History of Phreatic Eruptions in the Noboribetsu Geothermal Field, Kuttara Volcano, Hokkaido, Japan

Yoshihiko GOTO*, Hirotaka SASAKI*, Yoshimasa TORIGUCHI* and Akira HATAKEYAMA*

(Received December 12, 2012; Accepted July 18, 2013)

A 6.3-m-deep trench was dug in the Noboribetsu Geothermal Field, Kuttara Volcano, Hokkaido, Japan, to clarify the history of phreatic eruptions in the field. The stratigraphic section in the trench consists of (from lower to upper): the Kt-1 pyroclastic surge deposit, nine phreatic fall deposits (Nb-l to Nb-d), the B-Tm tephra, two phreatic fall deposits (Nb-c, Nb-b), the Us-b tephra, and a phreatic fall deposit (Nb-a). The 12 phreatic fall deposits (Nb-l to Nb-a) are 3–100 cm thick and consist of altered dacitic lithic fragments in a clay-rich fine-grained matrix. These deposits are inferred to have been erupted from the Noboribetsu Geothermal Field. Buried soil layers occur between the deposits. Radiocarbon dating of buried soil samples from immediately below each of the phreatic fall deposits suggests that phreatic eruptions occurred at *ca.* BC 6450, BC 5370, BC 3980, BC 3440, BC 1990, BC 1710, BC 1280, BC 900, BC 200, AD 980, AD 1480, and after AD 1663, corresponding to an average eruption interval of ~ 700 years.

Key words: eruptive history, phreatic explosion, Noboribetsu Geothermal Field, Kuttara Volcano, trench survey

1. Introduction

Geothermal fields are common in active volcanic regions and have become major sites for tourism and for extracting geothermal energy. Although there have been few historical volcanic eruptions in geothermal fields, geological studies suggest that phreatic eruptions (here, the term ‘phreatic eruptions’ is used for steam-driven explosions that do not involve fresh magma, following Barberi *et al.*, 1992 and McPhie *et al.*, 1993) in such settings occur at intervals of 100–1000 years (Lloyd, 1972; Hedenquist and Henley, 1985; Ito, 1999; Kudo *et al.*, 2000; Miyabuchi and Watanabe, 2000; Browne and Lawless, 2001; Okuno, 2002; Ohba and Kitade, 2005; Kobayashi *et al.*, 2006; Mannen, 2007). Therefore, an understanding of the eruptive history of a geothermal field is essential in evaluating the volcanic hazard in the region.

The Noboribetsu Geothermal Field at Kuttara Volcano, southwestern Hokkaido (Fig. 1), is one of the major geothermal fields in Japan. The existence of small explosion craters in this field suggests that phreatic eruptions have occurred in recent geological time (Yamazaki, 1986; Katsui *et al.*, 1988; Goto *et al.*, 2011a, 2011b). However, the history of eruptions remains unknown, because this field is generally covered with thick vegetation, and there are few exposures of phreatic deposits. To address this shortcoming, we conducted a trench survey and performed radiocarbon dating of phreatic deposits erupted from the field. This paper reports on the stratigraphy and radio-

carbon ages of the phreatic deposits and discusses the eruptive history of the geothermal field.

2. Noboribetsu Geothermal Field

The Noboribetsu Geothermal Field lies in the western part of Kuttara Volcano (Fig. 1), an andesitic to rhyolitic composite volcano (elevation, 549 m above sea level) with a small caldera at its summit (Lake Kuttara). The volcano evolved over the period 80–45 ka, involving early silicic explosive activity and subsequent stratovolcano building associated with caldera collapse at about 40 ka (Katsui *et al.*, 1988; Yamagata, 1994; Moriizumi, 1998; Moriya, 2003). The geothermal field, which is inferred to have formed after the collapse of the caldera (Katsui *et al.*, 1988), is approximately 1 km wide (NE–SW) and 1.5 km long (NW–SE).

The Noboribetsu Geothermal Field is characterized by a dacitic cryptodome (Hiyoriyama Cryptodome), a volcanic lake (Oyunuma Lake), and a fumarolic valley (Jigokudani Valley) (Fig. 2). The Hiyoriyama Cryptodome, located in the northern part of the geothermal field, is 350–550 m in diameter and rises 130 m above the surrounding area (Fig. 3; Goto *et al.*, 2011a). Fission-track analyses indicate that the dome formed at 15 ± 3 ka (Goto and Danhara, 2011). Oyunuma Lake (115 × 210 m in area), located in the central part of the geothermal field, is the largest lake in the field and is filled with hot acidic water (Fig. 3). The Jigokudani Valley, in the southern part of the geothermal

*College of Environmental Technology, Graduate School of Engineering, Muroran Institute of Technology, Mizumoto-cho 27-1, Muroran, Hokkaido 050-8585, Japan

Corresponding author: Yoshihiko Goto
e-mail: ygoto@mmm.muroran-it.ac.jp

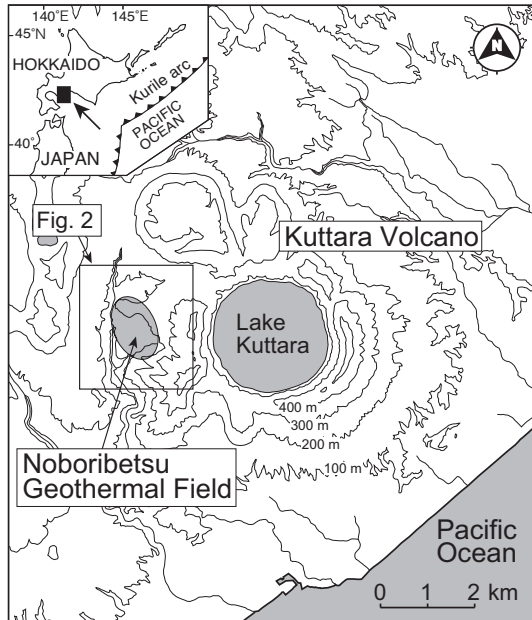


Fig. 1. Location of the Noboribetsu Geothermal Field in the western part of Kuttara Volcano, southwestern Hokkaido, Japan. Topographic contour interval is 100 m.

field, extends for 500 m in an ENE–WSW orientation and hosts active fumaroles. The geothermal manifestations of the geothermal field (active fumaroles, hot springs, and hydrothermal alteration zones) are distributed in a zone extending NNW–SSE from the Hiyoriyama Cryptodome to the Jigokudani Valley (Goto and Johmori, 2011).

3. Phreatic fall deposits of the Noboribetsu Geothermal Field

Phreatic fall deposits, extruded from the Noboribetsu Geothermal Field, are widely distributed over the field (Yamazaki, 1986; Katsui *et al.*, 1988; Goto *et al.*, 2011b). They occur above the Kt-1 pyroclastic surge deposit (Moriizumi, 1998) or the Kt-1 pyroclastic flow deposit (Moriizumi, 1998), both of which were extruded from Kuttara Volcano at about 40 ka. In previous studies, the phreatic fall deposits have been named the Oyunuma-Jogokudani explosion deposits (Yamazaki, 1986), the Shinki-Jigokudani pyroclastic fall deposit (Katsui *et al.*, 1988), or the Hiyoriyama phreatic deposit (Goto *et al.*, 2011b). Here, these deposits are referred to as the Noboribetsu phreatic fall deposits, to avoid confusion. These deposits comprise 12 units, ranging from the uppermost Noboribetsu-a phreatic fall deposit (Nb-a) to the lowermost Noboribetsu-l phreatic fall deposit (Nb-l deposit), as described below. The relations between the Noboribetsu phreatic fall deposits and the previously reported phreatic deposits are described in section 7–2.

4. Trench survey

Stratigraphic and geochronological studies of the Noboribetsu phreatic fall deposits are hampered by limited exposure due to thick vegetation cover in the Noboribetsu Geothermal Field. We conducted a trench survey of the deposits to determine the stratigraphic record of eruption events and to collect buried soil samples for radiocarbon dating. The trench was excavated upon a gentle ridge located 200 m northeast of Oyunuma Lake (Fig. 2). This site was chosen because the lake is the largest and most centrally located explosion crater in the Noboribetsu Geothermal Field. The area around the trench site is covered with tall trees and short bamboo forest (Fig. 3). The trench was excavated on 24–25 November 2005 using a backhoe with a 0.3 m³ bucket. The trench was 3.5 m wide, 7.0 m long, and 6.3 m deep (Fig. 4). The long axis of the trench was oriented east–west.

5. Geological section in the trench

The stratigraphic section in the trench consists of a subhorizontal sequence comprising (from lower to upper) the Kt-1 pyroclastic surge deposit, the Nb-1 to Nb-d deposits, the B-Tm tephra (Machida and Arai, 2003), the Nb-c deposit, the Nb-b deposit, the Us-b tephra (Yokoyama *et al.*, 1973), and the Nb-a deposit (Figs. 4 and 5). Buried soil layers (0.5–5.0 cm thick) occur between each of these units.

The Kt-1 pyroclastic surge deposit (> 71 cm thick) is brown (Munsell color chart 10YR 4/4), thinly bedded, coarse grained (1–2 mm), and composed of lithic fragments, mineral fragments (plagioclase, quartz, hypersthene, augite, hornblende, opaque minerals), and fresh volcanic glass. The deposit contains abundant accretionary lapilli (< 5 mm across). The refractive index of the volcanic glass ranges from 1.4961 to 1.5031 (mean, 1.499; mode, 1.499; as analyzed using RIMS2000 machine at Kyoto Fission-Track Co., Ltd, Japan, following the method of Danhara *et al.*, 1992). This deposit is overlain by a brown (10YR 4/3) soil layer (5 cm thick).

The Nb-1 deposit (70 cm thick) is bright brown (7.5YR 5/8), massive (non-stratified), matrix supported, poorly sorted, and composed of subrounded to subangular, dacitic lithic clasts (< 30 cm across) in a fine-grained matrix (Fig. 4). The clasts are pale brown to pale grey, and intensely altered. The matrix is clay-rich, cohesive, and composed of altered dacite fragments, mineral fragments (plagioclase, quartz, hornblende, hypersthene, augite, opaque minerals), and weathered volcanic glass. The grain-size distribution of the deposit shows a relatively even spread from –7 to 4 ϕ (Fig. 6L). X-ray diffraction (XRD) analysis of the < 2 μ m fraction (separated by hydraulic elutriation) indicates the presence of gypsum, pyrophyllite, epidote, and vermiculite (Table 1). This deposit is overlain by a brown (10YR 4/3) soil layer (1 cm thick).

The Nb-k deposit (60 cm thick) is light yellow (2.5Y

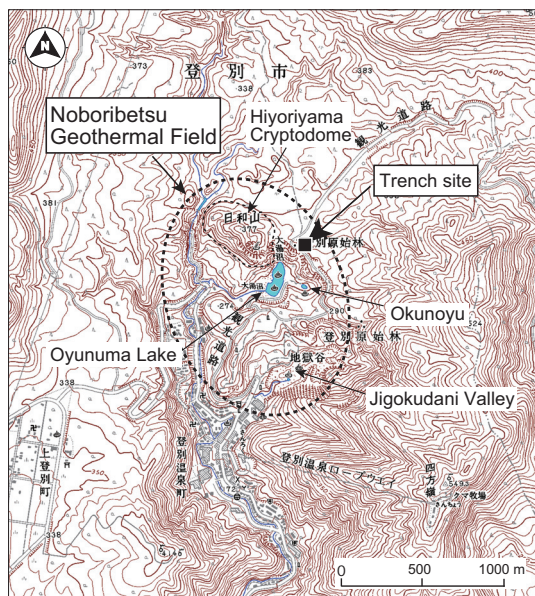


Fig. 2. Topographic map of the Noboribetsu Geothermal Field, showing the location of the trench site. The trench was excavated 200 m northeast of Oyunuma Lake, which is the largest explosion crater in the geothermal field. The base map is after the 1:25,000 scale topographic map 'Noboribetsu-Onsen' issued by the Geospatial Information Authority of Japan (GSI). Topographic contour interval is 10 m.

7/4), massive, and composed of subrounded to subangular, dacitic lithic clasts (< 10 cm across) in a fine-grained matrix (Fig. 4). The clasts are pale grey and intensely altered. Some clasts show an impact sag structure onto the underlying soil layer. The matrix is clay-rich, cohesive, and composed of altered dacite fragments, mineral fragments (plagioclase, quartz, hypersthene, hornblende, augite, opaque minerals), and weathered volcanic glass. The grain size of the deposit is mainly smaller than 4ϕ (Fig. 6K). XRD analysis of the < $2\mu\text{m}$ fraction (Table 1) indicates the presence of smectite, gypsum, and epidote. This deposit is overlain by a brown (10YR 4/3) soil layer (0.5 cm thick).

The Nb-j deposit (65 cm thick) is bright brown (7.5YR 5/8), massive, and composed of subrounded to subangular, dacitic lithic clasts (< 30 cm across) in a fine-grained matrix (Fig. 4). The clasts are pale brown to pale grey, and intensely altered. The matrix is clay-rich, cohesive, and composed of altered dacite fragments, mineral fragments (plagioclase, quartz, hypersthene, augite, hornblende, biotite, opaque minerals), and weathered volcanic glass. This deposit contains charcoal fragments (< 4 mm across). The grain size distribution of the deposit shows a dominance of grains smaller than 4ϕ (Fig. 6J). XRD analysis of the < $2\mu\text{m}$ fraction (Table 1) indicates the presence of gypsum

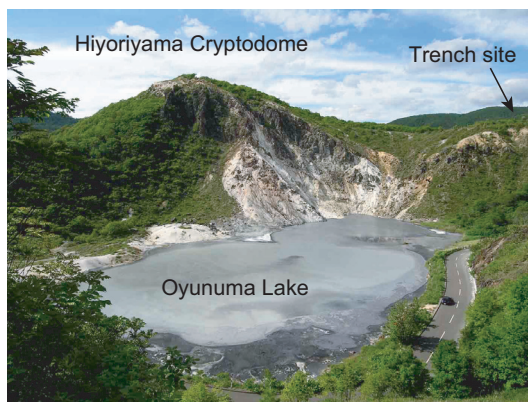


Fig. 3. Photograph of the Hiyoriyama Cryptodome and Oyunuma Lake in the Noboribetsu Geothermal Field (viewed from the south), showing the trench site.

and quartz. This deposit is overlain by a dark brown (10YR 2/2) soil layer (0.5 cm thick).

The Nb-i deposit (20 cm thick) is bright brown (7.5YR 5/8), massive, and composed of subrounded to subangular, dacite clasts (< 30 cm across) in a fine-grained matrix (Fig. 4). The clasts are pale brown to pale grey, and intensely altered. The matrix is clay-rich, cohesive, and composed of altered dacite fragments, mineral fragments (plagioclase, quartz, hypersthene, augite, hornblende, biotite, opaque minerals), and weathered volcanic glass. Grain-size analysis shows a dominance of grains smaller than 4ϕ (Fig. 6I). XRD analysis of the < $2\mu\text{m}$ fraction (Table 1) indicates the presence of smectite, gypsum, and quartz. This deposit is overlain by a dark brown (10YR 2/2) soil layer (1 cm thick).

The Nb-h deposit (3 cm thick) is brown (7.5YR 4/6), massive, and composed of subrounded, dacitic lithic clasts (1–5 cm across) and dacitic pumice clasts (1–2 cm across) in a fine-grained matrix (Fig. 4). All clasts are pale grey and intensely altered, and their color means they are conspicuous in the brown matrix. The matrix is clay-rich, cohesive, and composed of altered dacite fragments, mineral fragments (plagioclase, quartz, hypersthene, augite, hornblende, opaque minerals), and weathered volcanic glass. Grain-size analysis shows a bimodal grain-size distribution (Fig. 6H). XRD analysis of the < $2\mu\text{m}$ fraction (Table 1) indicates the presence of smectite, kaolinite, quartz, and opal. This deposit is overlain by a dark brown (10YR 2/2) soil layer (7 cm thick).

The Nb-g deposit (3 cm thick) is brown (10YR 4/6), massive, and composed of subrounded to subangular, dacitic lithic clasts (< 1 cm across) in a fine-grained matrix (Fig. 4). The clasts are pale brown to pale grey, and intensely altered. The matrix is clay-rich, cohesive, and composed of altered dacite fragments, mineral fragments (plagioclase, quartz, hypersthene, augite, hornblende,



Fig. 4. Photograph of the trench, showing the sequence of Noboribetsu phreatic fall deposits (Nb-a to Nb-l), the B-Tm tephra, and the Us-b tephra (viewed from the east). Buried soil layers occur between adjacent units. Note the impact sag structure at the bottom of the Nb-c deposit. The striped rod in the trench is 90 cm long (each colored segment is 10 cm long).

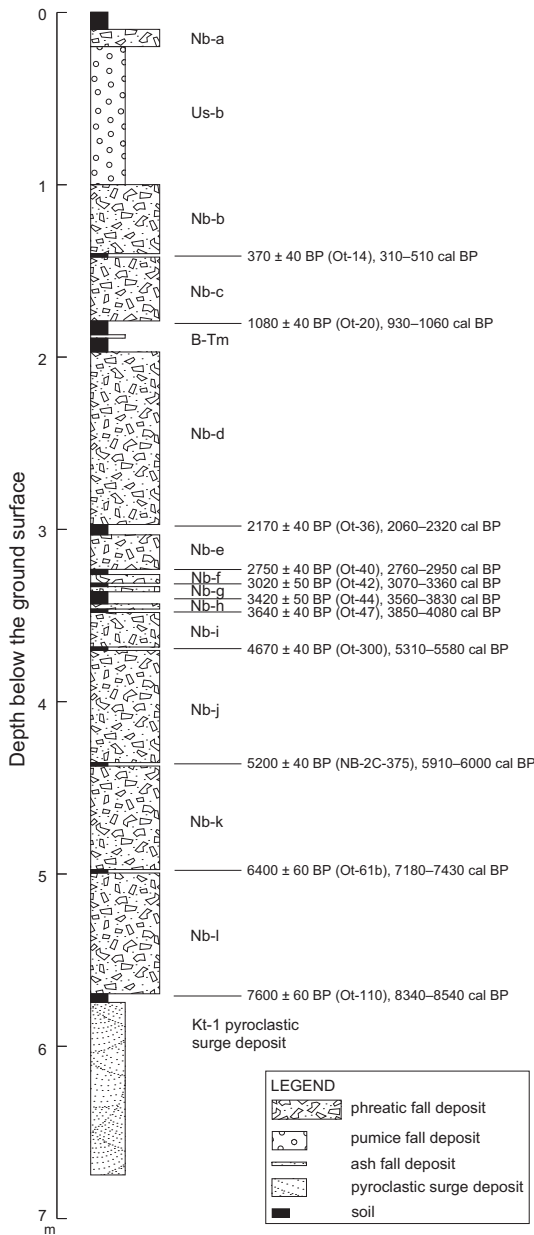


Fig. 5. Stratigraphic section in the trench. The section comprises the Noboribetsu phreatic fall deposits (Nb-a to Nb-l), the Kt-1 pyroclastic surge deposit (Kt-1), the B-Tm tephra, and the Us-b tephra. Buried soil layers occur between adjacent units. Radiocarbon ages (conventional ages) and calibrated ages (error range 2σ) are also shown.

opaque minerals), and weathered volcanic glass. This deposit contains many charcoal fragments (< 3 mm across). Grain-size analysis (Fig. 6G) shows a dominance of grains smaller than 4ϕ . XRD analysis of the $< 2\mu\text{m}$ fraction

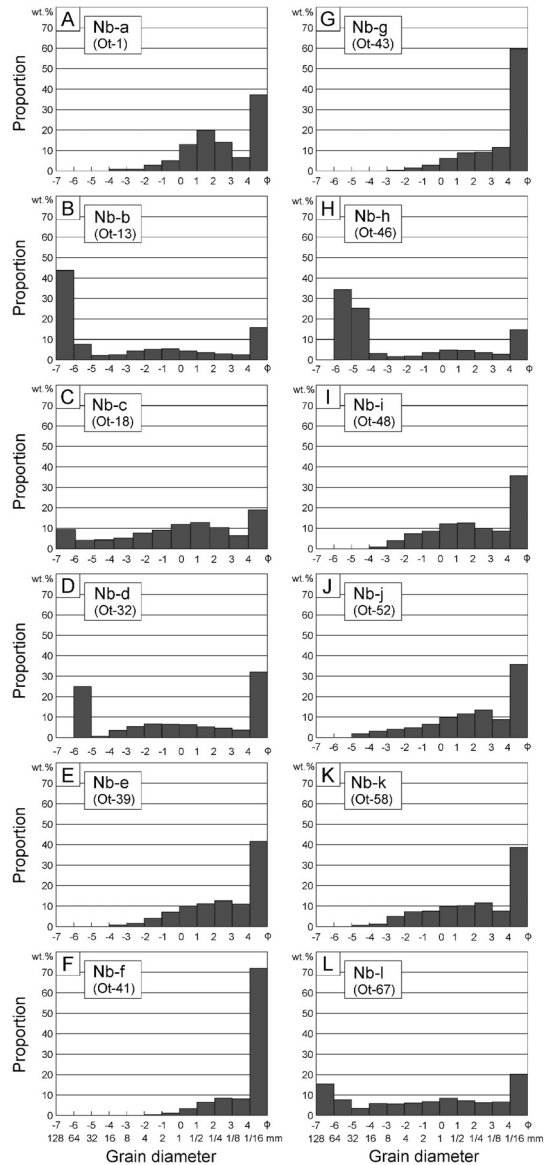


Fig. 6. Grain-size histograms of the Noboribetsu phreatic fall deposits (Nb-a to Nb-l) sampled from the trench. The deposits contain a large proportion of grains smaller than 4ϕ . The samples were sieved at mesh intervals of 1ϕ (where $\phi = -\log_2 d$, with d being the grain size in millimeters), using a set of sieves ranging from -7 to 4ϕ (128 mm to $1/16$ mm). The sieving was carried out in a water bath because the samples were cohesive. The sieved samples were dried and weighed to an accuracy of 0.01 g on a laboratory balance.

(Table 1) indicates the presence of smectite, kaolinite, quartz, and opal. This deposit is overlain by a dark brown

Table 1. Results of X-ray diffraction (XRD) analyses of the <2 mm fraction of the Noboribetsu phreatic fall deposits (Nb-a to Nb-l), sampled from the trench. The modal abundance of each mineral is classified as abundant (+++), moderate (++), or trace (+).

	Smectite	Kaolinite	Gypsum	Pyrophyllite	Jarosite	Illite	Epidote	Vermiculite	Quartz	Tridymite	Opal
Nb-a	+++	+++							++		
Nb-b	+++	+++		+	+	+			+		
Nb-c	++	+++	++								
Nb-d	+++	+++							+	++	++
Nb-e	+++	+++			+						
Nb-f	+++	++							+		+
Nb-g	+++	++							+		+
Nb-h	+++	++							+		+
Nb-i	+		+++						+		
Nb-j			+++						+		
Nb-k	+		+++					+			
Nb-l			+++	+			+	+			

The <2 mm fraction sample was separated by hydraulic elutriation and prepared as oriented samples on glass slides. The XRD analyses were carried out at Okayama University of Science, using a Geigerflex RAD-B diffractometer (Rigaku Corporation) with settings of 40 kV, 60 mA, and scan speed of 2.0° per minute. Ethylene glycol treatment was used to identify smectite.

(10YR 2/2) soil layer (2 cm thick).

The Nb-f deposit (5 cm thick) is yellowish brown (10YR 5/6), massive, and composed of subrounded to subangular, dacitic lithic clasts (<1 cm across) in a fine-grained matrix (Fig. 4). The clasts are pale brown to pale grey, and intensely altered. The matrix is clay-rich, cohesive, and composed of altered dacite fragments, mineral fragments (plagioclase, quartz, hypersthene, augite, hornblende, opaque minerals), and weathered volcanic glass. This deposit contains many charcoal fragments (<3 mm across). Grain-size analysis (Fig. 6F) shows a dominance of grains smaller than 4 ϕ . XRD analysis of the <2 μ m fraction (Table 1) indicates the presence of smectite, kaolinite, quartz, and opal. This deposit is overlain by a dark brown (10YR 2/2) soil layer (3 cm thick).

The Nb-e deposit (20 cm thick) is bright brown (7.5YR 5/8), massive, and composed of subrounded to subangular, dacitic lithic clasts (<10 cm across) in a fine-grained matrix (Fig. 4). The clasts are pale brown to pale grey, and intensely altered. The matrix is clay-rich, cohesive, and composed of altered dacite fragments, mineral fragments (plagioclase, quartz, hypersthene, augite, hornblende, opaque minerals), and weathered volcanic glass. Some clasts show an impact sag structure onto the underlying soil layer and also onto the Nb-f deposit beneath the soil layer. Grain-size analysis shows a dominance of grains smaller than 4 ϕ (Fig. 6E). XRD analysis of the <2 μ m fraction (Table 1) indicates the presence of smectite, kaolinite, and jarosite. This deposit is overlain by a dark brown (10YR 2/2) soil layer (6 cm thick).

The Nb-d deposit (100 cm thick) is light yellow (2.5Y 7/4), massive, and composed of subrounded to subangular, dacitic lithic clasts and minor andesitic lithic clasts (<80 cm across) in a fine-grained matrix (Fig. 4). The dacitic

lithic clasts are pale grey and intensely altered, whereas the andesitic lithic clasts are pale brownish grey and slightly altered. The matrix is clay-rich, cohesive, and composed of altered dacite fragments, mineral fragments (quartz, plagioclase, hypersthene, augite, hornblende, opaque minerals), and weathered volcanic glass. Some clasts show an impact sag structure onto the underlying soil layer and also onto the Nb-e deposit beneath the soil layer (Fig. 4). Grain-size analysis shows a bimodal grain-size distribution, with a dominance of grains smaller than 4 ϕ (Fig. 6D). XRD analysis of the <2 μ m fraction (Table 1) indicates the presence of smectite, kaolinite, quartz, tridymite, and opal. This deposit is overlain by a dark brown (10YR 2/2) soil layer (5 cm thick).

The B-Tm tephra (1 cm thick) is white (N9), fine-grained, and composed of fresh volcanic glass and crystals of K-feldspar, plagioclase, quartz, orthopyroxene, clinopyroxene, and opaque minerals (Fig. 4). The refractive index of the glass (as analyzed using RIMS2000 machine) shows a bimodal distribution, with one mode ranging from 1.5082 to 1.5145 (mean, 1.510; mode, 1.510; proportion of analyses, 58%) and the other from 1.5167 to 1.5217 (mean, 1.520; mode, 1.520; proportion of analyses, 42%). The refractive index is consistent with that of the B-Tm tephra reported by Machida and Arai (2003). The tephra is overlain by a dark brown (10YR 2/2) soil layer (4 cm thick).

The Nb-c deposit (37 cm thick) is reddish brown (5YR 4/8), massive, and composed of subrounded to subangular, dacitic lithic clasts (<20 cm across) in a fine-grained matrix (Fig. 4). The clasts are pale brown to pale grey, and intensely altered. The matrix is clay-rich, cohesive, and composed of altered dacite fragments, mineral fragments (quartz, plagioclase, hypersthene, augite, hornblende,

opaque minerals), and weathered volcanic glass. Some clasts show an impact sag structure onto the underlying soil layer and also onto the Nb-d deposit beneath the soil layer (Fig. 4). The grain-size distribution of the deposit shows a relatively even spread (Fig. 6C). XRD analysis of the $< 2 \mu\text{m}$ fraction (Table 1) indicates the presence of smectite, kaolinite, and gypsum. This deposit is overlain by a dark brown (10YR 2/2) soil layer (1 cm thick).

The Nb-b deposit (40 cm thick) is light yellow (2.5Y 7/3), massive, and composed of subrounded to subangular, dacitic lithic clasts (< 20 cm across) in a fine-grained matrix (Fig. 4). The clasts are pale brown to pale grey, and intensely altered. The matrix is clay-rich, cohesive, and composed of altered dacite fragments, mineral fragments (quartz, plagioclase, hypersthene, hornblende, biotite, augite, opaque minerals), and weathered volcanic glass. Some clasts show an impact sag structure onto the underlying soil layer. Grain-size analysis shows a bimodal grain-size distribution, with a dominance of grains smaller than 4ϕ (Fig. 6B). XRD analysis of the $< 2 \mu\text{m}$ fraction (Table 1) indicates the presence of smectite, kaolinite, pyrophyllite, jarosite, illite, and quartz. This deposit is directly overlain by the Us-b tephra.

The Us-b tephra (80 cm thick) is clast supported and poorly stratified, and consists of rhyolite pumice (1–3 cm across; Fig. 4). The pumice is white (N9) and consists of fresh volcanic glass and crystals of plagioclase, hypersthene, augite, hornblende, and opaque minerals. The refractive index of the volcanic glass ranges from 1.4887 to 1.4921 (mean, 1.491; mode, 1.491; analyzed using RIMS2000 machine). This tephra is directly overlain by the Nb-a deposit.

The Nb-a deposit (10 cm thick) is olive brown (2.5Y 4/3), massive, and composed of subrounded to subangular, dacitic lithic clasts (< 1 cm across) in a fine-grained matrix (Fig. 4). The clasts are pale grey to grey, and intensely altered. The matrix is clay-rich, cohesive, and composed of altered dacite fragments, mineral fragments (quartz, plagioclase, hypersthene, hornblende, biotite, augite, opaque minerals), and weathered volcanic glass. Grain-size analysis shows a dominance of grains smaller than 4ϕ (Fig. 6A). XRD analysis of the $< 2 \mu\text{m}$ fraction (Table 1) indicates the presence of smectite, kaolinite, and quartz. This deposit is overlain by dark brown (10YR 2/2) surface soil (10 cm thick).

6. Radiocarbon dating

Radiocarbon ages were determined for 11 soil samples collected from buried soil layers located immediately below 11 of the phreatic fall deposits exposed in the trench (see Fig. 5). The soil layers contain no modern plant roots, and show no sign of disturbance (*e.g.*, bioturbation, erosion) during or after deposition. Each sample was collected from the uppermost 1 cm of the soil layer. In the case that a soil layer was less than 1 cm thick, the entire thickness of the

soil layer was used for dating. Each sample for dating consisted of dark brown or brown, organic sediment (grain size < 0.5 mm).

Radiocarbon dating was performed by Beta Analytic (Miami, USA). All samples were pretreated with acid washes, and the remaining carbon (bulk organic fraction) was analyzed for dating (Table 2). Eight samples (Ot-14, Ot-20, Ot-36, Ot-40, Ot-42, Ot-44, Ot-61b, Ot-110) were analyzed using a standard radiometric method, and three samples (Ot-47, Ot-300, NB-2C-375) were analyzed using an accelerator mass spectrometry (AMS) method (Table 2). The soil samples yield conventional radiocarbon ages of (from the lowermost to uppermost samples) 7600 ± 60 BP, 6400 ± 60 BP, 5200 ± 40 BP, 4670 ± 40 BP, 3640 ± 40 BP, 3420 ± 50 BP, 3020 ± 50 BP, 2750 ± 40 BP, 2170 ± 40 BP, 1080 ± 40 BP, and 370 ± 40 BP (BP = years before AD 1950; error range 1σ ; Table 2). These ages are consistent with the stratigraphic positions of the soils (Fig. 5).

Calibrated ages were calculated from the conventional radiocarbon ages, using a program developed by Beta Analytic and based on the IntCal09 calibration database (Oeschger *et al.*, 1975; Stuiver and Braziunas, 1993; Heaton *et al.*, 2009; Reimer *et al.*, 2009) with a spline smoothing function for the calibration curve (Talma and Vogel, 1993). The calibrated ages are (from the lowermost to uppermost samples) 8340–8540 cal BP (BC 6390–6590), 7180–7430 cal BP (BC 5230–5480), 5910–6000 cal BP (BC 3960–4050), 5310–5580 cal BP (BC 3360–3630), 3850–4080 cal BP (BC 1900–2140), 3560–3830 cal BP (BC 1610–1880), 3070–3360 cal BP (BC 1120–1410), 2760–2950 cal BP (BC 810–1000), 2060–2320 cal BP (BC 110–370), 930–1060 cal BP (AD 890–1020), and 310–510 cal BP (AD 1440–1640) (error range 2σ , 95 % probability; Table 2).

The calibrated ages are consistent with ages reported previously for the Kt-1 pyroclastic surge deposit (~ 40 ka; Moriizumi, 1998), the B-Tm tephra ($\sim 10^{\text{th}}$ century; Machida and Arai, 2003), and the Us-b tephra (AD 1663; Yokoyama *et al.*, 1973; Machida and Arai, 2003) (Fig. 5). The Nb-a deposit occurs above the Us-b tephra, suggesting it was deposited after AD 1663.

7. Discussion

7-1 Origin of the Noboribetsu phreatic fall deposits

The Noboribetsu phreatic fall deposits (Nb-l to Nb-a) consist of altered dacitic lithic clasts in an altered fine-grained matrix, and contain no juvenile magmatic pyroclasts, suggesting they were produced during phreatic explosions. The grain-size distributions of the deposits (which generally show a dominance of grains smaller than 4ϕ) and the presence of clay minerals (*e.g.*, smectite and kaolinite; Table 1) are consistent with the deposits originating during a phreatic explosion. The presence of large lithic clasts (up to 80 cm across) and impact sag structures suggests that the deposits were erupted from

Table 2. Radiocarbon ages of buried soils collected from the trench.

Sample number	Material	Method	^{14}C age* (BP, $\pm 1\sigma$)	$\delta^{13}\text{C}$ (permil)	Conventional ^{14}C age** (BP, $\pm 1\sigma$)	Lab code Beta-	Calibrated result*** (cal BP)	(cal AD/BC)
Ot-14	organic sediment (bulk organic fraction)	radiometric	400 \pm 40	-26.7	370 \pm 40	211989	310-510 (2 σ) 470 (intercept)	AD 1440-1640 (2 σ) AD 1480 (intercept)
Ot-20	organic sediment (bulk organic fraction)	radiometric	1090 \pm 40	-25.8	1080 \pm 40	211990	930-1060 (2 σ) 970 (intercept)	AD 890-1020 (2 σ) AD 980 (intercept)
Ot-36	organic sediment (bulk organic fraction)	radiometric	2150 \pm 40	-23.6	2170 \pm 40	211991	2060-2320 (2 σ) 2150 (intercept)	BC 110-370 (2 σ) BC 200 (intercept)
Ot-40	organic sediment (bulk organic fraction)	radiometric	2760 \pm 40	-26.0	2750 \pm 40	211992	2760-2950 (2 σ) 2850 (intercept)	BC 810-1000 (2 σ) BC 900 (intercept)
Ot-42	organic sediment (bulk organic fraction)	radiometric	3020 \pm 50	-25.0	3020 \pm 50	211993	3070-3360 (2 σ) 3220; 3230; 3240 (intercept)	BC 1120-1410 (2 σ) BC 1270; 1280; 1290 (intercept)
Ot-44	organic sediment (bulk organic fraction)	radiometric	3410 \pm 50	-24.0	3420 \pm 50	211994	3560-3830 (2 σ) 3640; 3660; 3690 (intercept)	BC 1610-1880 (2 σ) BC 1700; 1710; 1740 (intercept)
Ot-47	organic sediment (bulk organic fraction)	AMS	3620 \pm 40	-23.9	3640 \pm 40	217631	3850-4080 (2 σ) 3930; 3940; 3970 (intercept)	BC 1900-2140 (2 σ) BC 1980; 1990; 2020 (intercept)
Ot-300	organic sediment (bulk organic fraction)	AMS	4680 \pm 40	-25.7	4670 \pm 40	217630	5310-5480; 5540-5580 (2 σ) 5330; 5390; 5400; 5450 (intercept)	BC 3360-3530; 3590-3630 (2 σ) BC 3380; 3440; 3450; 3500 (intercept)
NIB2C-375	organic sediment (bulk organic fraction)	AMS	5170 \pm 40	-23.0	5200 \pm 40	249204	5910-6000 (2 σ) 5930 (intercept)	BC 3960-4050 (2 σ) BC 3980 (intercept)
Ot-61b	organic sediment (bulk organic fraction)	radiometric	6330 \pm 60	-21.0	6400 \pm 60	211995	7180-7190; 7250-7430 (2 σ) 7320 (intercept)	BC 5230-5240; 5300-5480 (2 σ) BC 5370 (intercept)
Ot-110	organic sediment (bulk organic fraction)	radiometric	7570 \pm 60	-22.8	7600 \pm 60	211996	8340-8480; 8490-8520; 8530-8540 (2 σ) 8400 (intercept)	BC 6390-6530; 6540-6570; 6580-6590 (2 σ) BC 6450 (intercept)

* Based on Libby's half-life (5568 years), uncorrected by $\delta^{13}\text{C}$ values. Ages are expressed in BP (years before AD 1950) with an error range of 1σ . ** The conventional ^{14}C age includes $\delta^{13}\text{C}$ correction. Ages are expressed in BP with an error range of 1σ . Vienna Pee Dee belemnite (VPDB) standard was used for $\delta^{13}\text{C}$ analysis. *** Calibrated ages were calculated from the conventional ^{14}C ages. Ages are expressed in cal BP and cal BC/AD with an error range of 2σ (95 % probability). Intercept ages with the calibration curve are also shown. AMS = accelerator mass spectrometry. The stratigraphic positions of the samples are shown in Fig. 5.

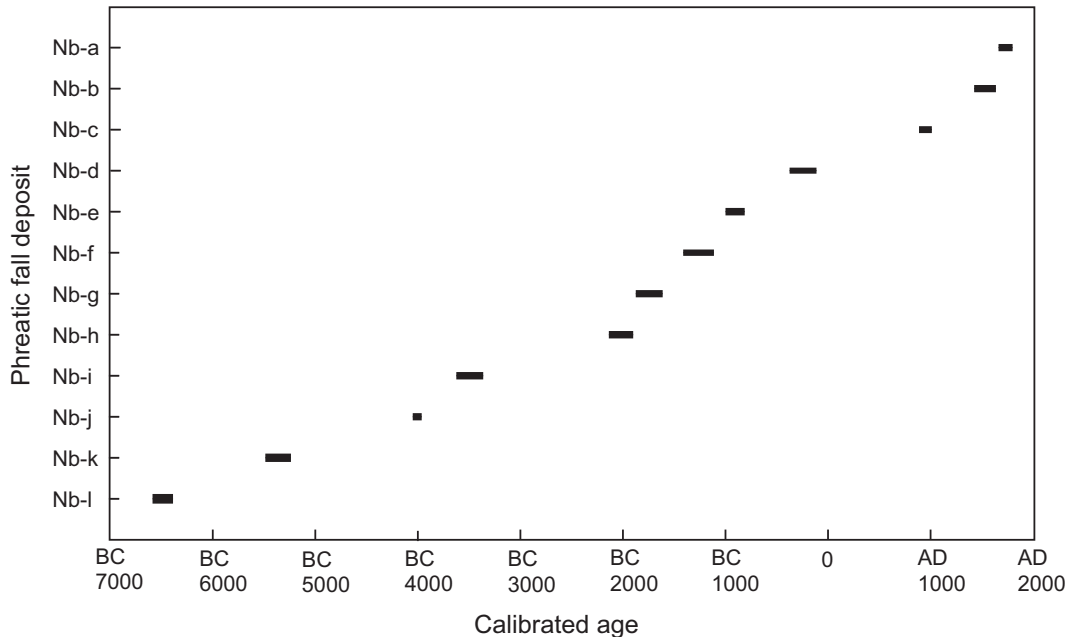


Fig. 7. Timing of phreatic eruptions in the Noboribetsu Geothermal Field. The width of each bar represents 2σ (95% probability).

within the Noboribetsu Geothermal Field, which is consistent with the presence of many small explosion craters in the field (Goto *et al.*, 2011a).

The 12 phreatic deposits (Nb-l to Nb-a) and intervening soil layers indicate the occurrence of 12 phreatic eruptions separated by periods of dormancy. The trench survey was performed at only one location, and it is possible that more than 12 phreatic fall deposits are present in the Noboribetsu Geothermal Field. We therefore conclude that at least 12 episodes of phreatic eruptions have occurred in the Noboribetsu Geothermal Field.

Since the trench survey gives only a one-dimensional perspective, the spatial distribution of each deposit (Nb-l to Nb-a) remains unknown; consequently, it is not possible to accurately estimate the volume of each deposit. The thicknesses of the deposits (maximum 100 cm, Nb-d) suggest that each phreatic eruption was relatively large in magnitude. We roughly estimate that the volume of each deposit is on the order of 10^5 m³.

7-2 Relations between the Noboribetsu phreatic fall deposits and previously reported phreatic deposits

Some of the Noboribetsu phreatic fall deposits (Nb-l to Nb-a) have been reported previously (Yamazaki, 1986; Katsui *et al.*, 1988; Goto *et al.*, 2011b). Yamazaki (1986) noted a set of phreatic fall deposits (the Oyunuma-Jogokudani explosion deposits) from 200 m east of Oyunuma Lake. The deposits are 5.6 m thick in total and comprise 10 units. Each unit is 5–150 cm thick and consists of dacitic

lithic clasts in a clay-rich, fine-grained matrix. Three buried soil layers occur between the units, and one soil layer was dated as 1880 ± 100 BP by radiocarbon methods. Yamazaki (1986) inferred that the deposits formed by phreatic eruptions within the Noboribetsu Geothermal Field. The 10 units may correspond to most of the Nb-l to Nb-a deposits, but detailed correlations between them are difficult, because the 10 units were poorly described and the radiocarbon age (1880 ± 100 BP) does not match our age data. The outcrop examined by Yamazaki (1986) is no longer accessible because it is covered by cement.

Katsui *et al.* (1988) described a phreatic fall deposit (the Shinki-Jigokudani pyroclastic fall deposit) from the southern part of the Noboribetsu Geothermal Field. The deposit occurs above the Us-b tephra, and consists of altered, dacitic lithic clasts in a fine-grained matrix. Katsui *et al.* (1988) inferred that the deposit formed during a small phreatic eruption within the Jigokudani Valley after AD 1663. Goto *et al.* (2011b) reported a phreatic fall deposit (the Hiyoriyama phreatic deposit) from the northern part of the Noboribetsu Geothermal Field. The deposit also occurs above the Us-b tephra and consists of fresh to altered, dacitic lithic clasts in a fine-grained matrix. Goto *et al.* (2011b) inferred that the deposit formed during a small phreatic eruption at the summit of the Hiyoriyama Cryptodome after AD 1663. The stratigraphic location (i.e., above the Us-b tephra) of these two deposits suggests that they correspond to the Nb-a deposit. The two deposits (i.e., the Nb-a deposit) are inferred to have been produced by

distinct phreatic explosions during a series of multiple-vent-forming phreatic explosions within an eruptive episode (Goto *et al.*, 2011b).

7-3 History of phreatic eruptions in the Noboribetsu Geothermal Field

The radiocarbon age of a buried soil located immediately below a mass-flow or pyroclastic deposit may represent the emplacement age of the deposit, in the case that the deposit overlies the soil without any disturbance (Orlova and Panychev, 1993; Okuno *et al.*, 1997; Xu *et al.*, 2004). In the present study, the soil layers show no sign of disturbance, suggesting the radiocarbon age of each soil represents the emplacement age of the overlying deposit. The calibrated ages (intercept ages; Table 2) suggest that phreatic eruptions occurred in the Noboribetsu Geothermal Field at *ca.* BC 6450 (Nb-l), BC 5370 (Nb-k), BC 3980 (Nb-j), BC 3440 (Nb-i), BC 1990 (Nb-h), BC 1710 (Nb-g), BC 1280 (Nb-f), BC 900 (Nb-e), BC 200 (Nb-d), AD 980 (Nb-c), AD 1480 (Nb-b), and after AD 1663 (Nb-a) (Fig. 7). The average interval between eruptions is ~ 700 years (*i.e.*, 12 eruptions in the past 8500 years), and the intervals range from 300 to 1400 years.

Considering the emplacement age of the Hiyoriyama Cryptodome (*ca.* 15 ka; Goto and Danhara, 2011), the 12 phreatic eruptions occurred after the emplacement of the dome. We suggest that the Noboribetsu Geothermal Field has an eruption history of dome emplacement at about 15 ka and phreatic eruptions after BC 6450 (or 8400 cal BP). The formation of the Hiyoriyama Cryptodome is the only magmatic event during the evolution of the Noboribetsu Geothermal Field (Katsui *et al.*, 1988), and the eruption history in this field is characterized by an early magmatic activity and later phreatic activity. Such an eruption history could be explained by early magma ascent followed by the repeated ascent of high-temperature volcanic fluid from depth.

A similar eruption history (*i.e.*, early dome-forming magmatic activity and later phreatic activity) has been reported for other geothermal fields (*e.g.*, the Owakudani area, Hakone Volcano, central Japan; Kobayashi *et al.*, 2006; Mannen, 2007). In the Owakudani area, a lava dome (Mt. Kanmurigatake) formed at about 3000 years ago, followed by at least five phreatic eruptions (Kobayashi *et al.*, 2006; Mannen, 2007). The frequency of phreatic eruptions in the Owakudani area (*i.e.*, 5 eruptions in the past 3000 years; Kobayashi *et al.*, 2006; Mannen, 2007) is also similar to that in the Noboribetsu Geothermal Field (12 eruptions in the past 8500 years; this study). The present results are therefore of value in evaluating the volcanic hazard in the Noboribetsu Geothermal Field.

Acknowledgements

This research was sponsored by the Ministry of Education, Culture, Sports, Science and Technology of Japan (MEXT), and supported financially by the Muroan

Institute of Technology. We thank the Ministry of the Environment, Japan, for granting permission for the trench survey. We thank T. Danhara (Kyoto Fission-Track Co. Ltd) for measuring the refractive index of volcanic glass. We are grateful to K. Mannen (Hot Springs Research Institute of Kanagawa Prefecture) and T. Ohba (Akita University) for reviewing the manuscript. Part of this work was performed as a component of compiling a hazard map for the City of Noboribetsu.

References

- Barberi, F., Bertagnini, A., Landi, P. and Principe, C. (1992) A review on phreatic eruptions and their precursors. *J. Volcanol. Geotherm. Res.*, **52**, 231–246.
- Browne, P.R.L. and Lawless, J.V. (2001) Characteristics of hydrothermal eruptions, with examples from New Zealand and elsewhere. *Earth-Science Reviews*, **52**, 299–331.
- Danhara, T., Yamashita, T., Iwano, H. and Kasuya, M. (1992) An improved system for measuring refractive index using the thermal immersion method. *Quaternary International*, **13/14**, 89–91.
- Goto, Y. and Danhara, T. (2011) Zircon fission-track dating of the Hiyoriyama Cryptodome at Kuttara Volcano, southwestern Hokkaido, Japan. *Bull. Volcanol. Soc. Japan*, **56**, 19–23.
- Goto, Y. and Johmori, A. (2011) Controlled source audio-frequency magnetotelluric (CSAMT) and time domain electromagnetic (TDEM) resistivity measurements at Noboribetsu Geothermal Field, Kuttara Volcano, Hokkaido, Japan. *Bull. Volcanol. Soc. Japan*, **56**, 153–160.
- Goto, Y., Matsuzuka, S. and Kameyama, S. (2011a) Three-dimensional digital mapping of Noboribetsu Geothermal Field, Kuttara Volcano, Hokkaido, Japan, using helicopter-borne high-resolution laser scanner. *Bull. Volcanol. Soc. Japan*, **56**, 127–135.
- Goto, Y., Sasaki, H., Toriguchi, Y. and Hatakeyama, A. (2011b) Phreatic explosion after AD 1663 at the Hiyoriyama Cryptodome, Kuttara Volcano, southwestern Hokkaido, Japan. *Bull. Volcanol. Soc. Japan*, **56**, 147–152.
- Heaton, T. J., Blackwell, P. G. and Buck, C. E. (2009) A Bayesian approach to the estimation of radiocarbon calibration curves: the Intcal09 methodology. *Radiocarbon*, **51**, 1151–1164.
- Hedenquist, J. W. and Henley, R. W. (1985) Hydrothermal eruptions in the Waiotapu Geothermal System, New Zealand: their origin, associated breccias, and relation to previous metal mineralization. *Econ. Geol.*, **80**, 1640–1668.
- Ito, J. (1999) Eruption sequence and ^{14}C ages of phreatic eruptions occurred at West-Iwate Volcano in historic age. *Bull. Volcanol. Soc. Japan*, **44**, 261–266. (in Japanese with English abstract)
- Katsui, Y., Yokoyama, I., Okada, H., Abiko, T. and Muto, H. (1988) **Kuttara (Hiyoriyama), its volcanic geology, history of eruption, present state of activity and prevention of disasters**. Committee for Prevention and Disasters of Hokkaido, Sapporo, 99p. (in Japanese)
- Kobayashi, M., Mannen, K., Okuno, M., Nakamura, T. and

- Hakamata, K. (2006) The Owakudani tephra group: a newly discovered post-magmatic eruption product of Hakone volcano, Japan. *Bull. Volcanol. Soc. Japan*, **51**, 245–256. (in Japanese with English abstract)
- Kudo, T., Okuno, M., Ohba, T., Kitade, Y. and Nakamura, T. (2000) The eruptive products from Jigoku-numa hot pool in Kita-Hakkoda volcano group, northeast Japan: eruption style, magnitude and age. *Bull. Volcanol. Soc. Japan*, **45**, 315–322. (in Japanese with English abstract)
- Lloyd, E. F. (1972) **Geology and hot springs of Orakeikorako**. New Zealand Geol. Survey Bull., 85, 164p.
- Machida, H. and Arai, F. (2003) **Atlas of Tephra in and around Japan**. University of Tokyo Press, Tokyo, 360p. (in Japanese)
- Mannen, K. (2007) Recent activities of Hakone volcano. In *National park geological leaflet 1, Hakone volcano* (The Geol. Soc. Japan ed.), The Geol. Soc. Japan. (in Japanese)
- McPhie, J., Doyle, M. and Allen, R. (1993) **Volcanic textures**. University of Tasmania, Hobart, 196p.
- Miyabuchi, Y. and Watanabe, K. (2000) Phreatic explosions and ejecta around Jigoku spa, southwestern part of the central cones of Aso volcano, Japan, *Bull. Volcanol. Soc. Japan*, **45**, 25–32. (in Japanese with English abstract)
- Moriizumi, M. (1998) The growth history of the Kuttara volcanic group. *Bull. Volcanol. Soc. Japan*, **43**, 95–111. (in Japanese with English abstract)
- Moriya, I. (2003) Kuttara volcano. In *Regional Geomorphology of the Japanese Islands, vol. 2, Geomorphology of Hokkaido* (Koaze, T., Nogami, M., Ono, Y. and Hirakawa, K. eds.), 279–281, University of Tokyo Press, Tokyo. (in Japanese)
- Oeschger, H., Siegenthaler, U., Schotterer, U. and Gugelmann, A. (1975) A box diffusion model to study the carbon dioxide exchange in nature. *Tellus*, **27**, 168–192.
- Ohba, T. and Kitade, Y. (2005) Subvolcanic hydrothermal systems: Implications from hydrothermal minerals in hydro-volcanic ash. *J. Volcanol. Geotherm. Res.*, **145**, 249–262.
- Okuno, M. (2002) Reconstruction of eruptive history of phreatic eruptions. *The Geographical Reports of Kanazawa University*, No. 10, 29–36. (in Japanese with English abstract)
- Okuno, M., Nakamura, T., Moriwaki, H. and Kobayashi, T. (1997) AMS radiocarbon dating of the Sakurajima tephra group, Southern Kyushu, Japan. *Nucl. Instr. Meth. Phys. Res.*, **B123**, 470–474.
- Orlova, L.A. and Panychev, V.A. (1993) The reliability of radiocarbon dating buried soils. *Radiocarbon*, **35**, 369–377.
- Reimer, P.J., Baillie, M.G.L., Bard, E., Bayliss, A., Beck, J. W., Blackwell, P.G., Ramsey, C.B., Buck, C.E., Burr, G.S., Edwards, R.L., Friedrich, M., Grootes, P.M., Guilderson, T. P., Hajdas, I., Heaton, T.J., Hogg, A.G., Hughen, K.A., Kaiser, K.F., Kromer, B., McCormac, F.G., Manning, S.W., Reimer, R.W., Richards, D.A., Southon, J.R., Talamo, S., Turney, C.S.M., Plicht, J. and Weyhenmeyer, C.E. (2009) Intcal 09 and Marine09 radiocarbon age calibration curves, 0–50,000 years cal BP. *Radiocarbon*, **51**, 1111–1150.
- Stuiver, M. and Braziunas, T.F. (1993) ^{14}C ages of marine samples to 10,000 BC. *Radiocarbon*, **35**, 137–189.
- Talma, A.S. and Vogel, J.C. (1993) A simplified approach to calibrating $\text{C}14$ dates. *Radiocarbon*, **35**, 317–322.
- Xu, S., Hoshizumi, H., Ochiai, Y., Aoki, H. and Uto, K. (2004) ^{14}C dating of soil samples from the Unzen volcano scientific drilling boreholes. *Nucl. Instr. Meth. Phys. Res.*, **B223–224**, 560–567.
- Yamagata, K. (1994) Tephrochronological study on the Shikotsu and Kuttara volcanoes in southwestern Hokkaido, Japan. *J. Geograph.*, **103**, 268–285. (in Japanese)
- Yamazaki, T. (1986) ^{14}C age of the Oyunuma-Jigokudani explosion deposits, Kuttara volcano, southwestern Hokkaido, Japan. *Earth Science (Chikyu Kagaku)*, **40**, 221–223. (in Japanese)
- Yokoyama, Katsui, Y., Oba, Y. and Ehara, Y. (1973) **Usuzan, its volcanic geology, history of eruption, present state of activity and prevention of disasters**. Committee for Prevention and Disasters of Hokkaido, Sapporo, 254p. (in Japanese)

(Editorial handling Mitsuhiro Yoshimoto)

北海道クッタラ火山，登別地熱地域の水蒸気噴火史

後藤芳彦・佐々木央岳・鳥口能誠・畠山 信

北海道クッタラ火山登別地熱地域，大湯沼の北東 200 m 地点において，トレンチ調査（深さ 6.3 m）を行い，登別地熱地域の噴火史を解明した。トレンチ断面の層序は，12 層の水蒸気噴火堆積物（厚さ 3-100 cm）と，それらに挟在する B-Tm テフラ，Us-b テフラからなる。12 層の水蒸気噴火堆積物は，変質したデイサイト質石質岩片（最大粒径 80 cm）と粘土質のマトリクスから構成され，サグ構造を示すことから，登別地熱地域から噴出したと考えられる。各々の水蒸気噴火堆積物は土壌層を挟在し，12 回の噴火が休止期を挟んで繰り返し起きたことを示す。水蒸気噴火堆積物の直下土壌層の放射性炭素年代測定値，および広域テフラとの対比により，水蒸気噴火は，約 BC6450 年，BC5370 年，BC3980 年，BC3440 年，BC1990 年，BC1710 年，BC1280 年，BC900 年，BC200 年，AD980 年，AD1480 年，および AD1663 年以降に起きたと推定される。登別地熱地域では，過去 8500 年間に 12 回以上の水蒸気噴火が起こり，噴火の頻度は 700 年に 1 回程度であると考えられる。